Viscoelastic shear properties of in vivo thigh muscles measured by MR elastography

Mashhour Chakouch, Philippe Pouletaut, Fabrice Charleux, Sabine Bensamoun

Viscoelastic Shear Properties of In Vivo Thigh Muscles Measured by MR Elastography

Mashhour K. Chakouch, PhD,[1] Philippe Pouletaut, PhD,[1] Fabrice Charleux, Dr,[2] and Sabine F. Bensamoun, PhD[1]*

Purpose: To measure the viscoelastic properties of passive thigh muscles using multifrequency magnetic resonance elastography (MMRE) and rheological models.
Materials and Methods: Four muscles in five volunteers underwent MMRE tests set up inside a 1.5T magnetic resonance imaging (MRI) scanner. Compression excitation was generated with a driver attached around the thigh, and waves were generated at 70, 90, and 110 Hz. In vivo experimental viscoelastic parameters ($\underline{G}(\omega) = G' + i\,G''$) were extracted from the wavelength and attenuation measurements along a local profile in the direction of the wave's displacement. The data-processing method was validated on a phantom using MMRE and RheoSpectris tests. The complex modulus ($\underline{G}(\omega)$) related to elasticity (μ) and viscosity (η) was then determined using four rheological models.
Results: Zener was the best-fit model ($\chi \sim 0.35$ kPa) for the rheological parameters of all muscles. Similar behaviors for the elastic components for each muscle were found for the Zener and springpot models. The gracilis muscle showed higher elastic values (about 2 kPa) in both models compared to other muscles. The α-values for each muscle was equivalent to the ratio G''/G' at 90 Hz.
Conclusion: MMRE tests associated with data processing demonstrated that the complex shear modulus $\underline{G}(\omega)$ of passive muscles could be analyzed using two rheological models. The viscoelastic data can be used as a reference for future assessment of muscular dysfunction.

J. MAGN. RESON. IMAGING 2015;00:000–000.

Noninvasive evaluation of the functional properties of soft tissues is important to clinicians when evaluating the behaviors of various tissues, such as muscle, brain, kidney, prostate, breast, and liver. MRE (magnetic resonance elastography) is a noninvasive medical imaging technique, developed from magnetic resonance imaging (MRI),[1,2] which can assess the shear elasticity of tissues by applying mechanical excitation. Motion-sensitive MR sequences are used to analyze the propagation of shear waves created by excitation through soft tissues.[3] MRE was applied to different healthy[4,5] and pathological soft tissues[1,6,7] to provide quantitative data.

The main mechanical property provided by the MRE technique used to be the shear modulus. MRE has been extensively improved and now provides reliable quantitative information on viscoelastic properties (eg, elasticity and viscosity),[8] which provide information on fluid and the solid components of soft tissues, which may be related to functional behavior. Thus, the viscoelastic properties of the brain,[9] muscle,[10] and liver[11] have been determined using multifrequency MRE (MMRE) tests to develop imaging sequences and reconstruction methods[12,13] that can visualize a clear propagation wave within tissues.

In addition, MMRE tests have been associated with rheological models, such as Voigt, Zener, and springpot. In the literature, the Voigt model is the main rheological model used to characterize viscoelastic behavior in soft tissues because of its simple composition.[14–16] The resulting wave images are analyzed by solving the inverse problem of elastography[17–19] to obtain the complex shear modulus (G). The storage modulus (G′), which represents the real part of the complex modulus, is determined by restoration of

View this article online at wileyonlinelibrary.com. DOI: 10.1002/jmri.25105

Received Aug 18, 2015, Accepted for publication Nov 10, 2015.

*Address reprint requests to: S.F.B., Université de Technologie de Compiègne (UTC), Centre de recherches de Royallieu, Laboratoire de BioMécanique et BioIngénierie, UMR CNRS 7338, Rue Personne de Roberval, BP 20529, Compiègne cedex, France. E-mail: sabine.bensamoun@utc.fr

From the [1]Biomechanics and Bioengineering Laboratory, UMR CNRS 7338, Sorbonne University, Université de Technologie de Compiègne, Compiègne, France; and [2]ACRIM-Polyclinique Saint Côme, Compiègne, France

mechanical energy because of the elastic properties of the material. The loss modulus (G″) represents the imaginary part of the complex modulus associated with its viscous properties according to the tissue's inherent mechanical friction which appears between the muscle fibers.[20] Both moduli (G′, G″) compose the viscoelastic properties.

In parallel to the in vivo MRE field of research, phantoms have been developed to realistically simulate the mechanical properties (elasticity, viscosity) of biological soft tissues: data obtained can contribute and improve the MRE protocol (frequency of excitation, inversion algorithms[21–23]). In the literature, multiple phantoms have been created with different compositions: agarose,[24] bovine,[25] Wirosil,[26] Plastisol,[27] zerdine hydrogel,[28] and copolymer-in-oil.[29] Multifrequency MRE tests can provide the viscoelastic properties of phantoms,[30] which are usually then validated using other mechanical techniques, such as rheometers.[31]

The main objective of this study was to measure the elasticity (G′) and viscosity (G″) parameters of individual passive thigh muscles (gracilis: Gr, semimembranosus: SM, semitendinosus: ST and biceps: BC) using multifrequency MRE and rheological models (Voigt, Maxwell, Zener, springpot). The secondary objective was to validate the in vivo data-processing using plastic phantoms that mimicked the muscles' viscoelastic properties under passive (rest) conditions.

Materials and Methods

Ethics statement

This study was approved by the Institutional Review Board of Amiens Hospital. All subjects had the experimental protocol explained and then gave their informed written consent prior to admission into the study.

Participants

The thigh muscles were studied in five healthy volunteers (three males, two females; age range: 21–38 years, mean age = 25 ± 5.32 years, BMI (body mass index) range: 19.4–28.4 $kg.m^{-2}$; mean BMI = 22.6 ± 3.1 $kg.m^{-2}$) with no muscle abnormality or histories of muscle disease.

Phantom Preparation

Large and a small cylindrical homogeneous phantoms were created for the MRE and spectroscopic techniques (mechanical test). Both phantoms were made with a mixture of a softener and liquid plastic (LureCraft, LaGrange, IN), or of Plastisol, which is a suspension of PVC particles in a plasticizer. The advantage of using Plastisol is being able to test objects with different elasticities, corresponding to different plastic concentrations, which are stable over time. In addition, Plastisol has a density close to that of soft tissue (1000 kg/m^3). Based on our previous studies,[32] the mixture was composed 50% plastic in order to create a medium with an elasticity close to that of muscle under a passive condition.

Then the mixtures were heated to 177°C[27] and the solutions were poured into large aluminum (diameter: 14 cm, height: 15 cm) and small aluminum molds (diameter: 9.9 mm, height: 76 mm). Because of the size of the small cylinder, the mold was placed on a glass slide in order to obtain a suitable surface on which the spectroscopy test could be performed. Both mixtures were left to cool and were stored at 23°C.

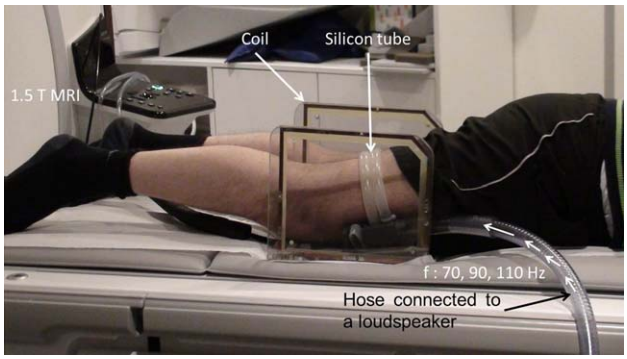

FIGURE 1: MRE setup placed inside a 1.5T MRI machine to measure the passive properties of the ischio (ST, SM, BC) and gracilis (Gr) muscles. Harmonic compression excitation was generated with a pneumatic driver (silicon tube) attached around the thigh muscles and waves were generated at 70, 90, and 110 Hz. ST: semitendinosus, SM: semimembranosus, BC biceps, Gr: gracilis.

Hyper-Frequency Viscoelastic Spectroscopy Tests

Hyper-frequency viscoelastic spectroscopy was performed using a RheoSpectris C500 instrument (Rheolution, Montreal, QC, Canada). This instrument is a new-generation viscoelastic spectroscope capable of measuring storage (G′) and loss (G″) moduli of materials across a wide range of frequencies between 10 and 1500 Hz. The basic principle of this instrument is to generate transient mechanical shear waves inside the probed sample, which is confined in a rigid cylindrical holder, and to measure the behavior (vibration) of the entire sample monitored at the surface, using an ultrasensitive optical sensor to process the viscoelastic spectroscopy.

For each measurement the small phantom within the cylindrical holder was placed in the mechanical unit that was specially designed to house the cylinders.[31] From viscoelastic measurements over the possible full-frequency range (10–500 Hz), only 60, 80, and 100 Hz were selected to compare with the MRE tests. Bland–Altman analysis was realized to compare the viscoelastic parameters between both tests.[33]

MRE Tests

MRE tests were conducted on the large phantom and on thigh muscles using a 1.5T Signa HDx MRI machine (General Electric, Milwaukee, WI).

MUSCLE CONFIGURATION. The subjects were placed in a prone position to characterize the ischio (ST, SM, BC, and Gr) muscles (Fig. 1). A custom-made Helmholtz surface coil was placed around the thigh and a pneumatic passive driver (silicon tube), consisting of a remote active pressure driver connected to a hose (tube), was wrapped and clamped around the subject's thigh. The tube was placed in the middle part of the thigh to investigate the ischio and gracilis muscles. Periodic variations in air pressure were induced into the tube at different frequencies: 70, 90, and 110 Hz.

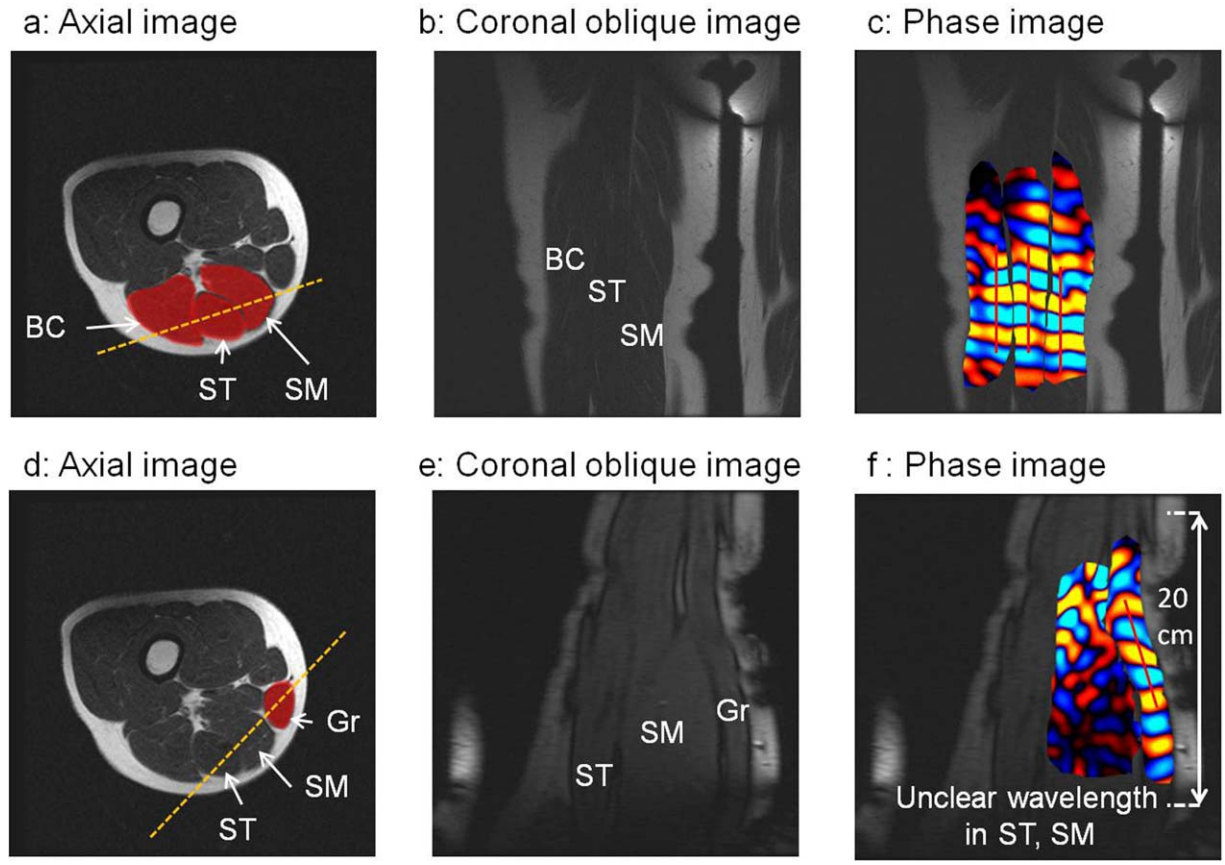

FIGURE 2: Illustration of the different steps to obtain the MRE phase images. a,d: Axial images of the thigh with placement of the imaging planes (dashed line) through the investigated muscle. b,e: Coronal oblique images of the muscles corresponding to the imaging planes. c,f: MMRE tests were performed on the coronal oblique image leading to acquisition of the phase images, representing displacement of the shear waves within the muscles. ST: semitendinosus, SM: semimembranosus, BC biceps, Gr: gracilis.

This caused acoustic waves to be propagated within the muscles. These frequencies were chosen as being optimal based on our previous MRE experiments on thigh muscles using this same tube driver.[10,27] The MRE pulse sequence included a sinusoidal motion-encoding gradient, which oscillated in the Z-direction at the same frequencies as the driver (70, 90, 110 Hz) and was used to image the coronal oblique plane of the displaced waves. In this study, the mechanical mode of excitation was a compression mode rather than a shear mode, as the energy of waves was more efficiently propagated throughout the muscles. Attenuation was less pronounced in the compression mode and more deep muscle shear waves were present.[34]

Anatomical axial images of the thigh muscle were acquired with a gradient-echo sequence. This used two oblique scouts on the medial side of the thigh: one that selected the ST, SM, and BC (Fig. 2a), and the other selected the Gr (Fig. 2d) muscle. This enabled coronal oblique images to reveal the entire muscle (ST, SM, BC, Gr) along the path of wave displacement along the thigh (Fig. 2c,f). Clear propagation, represented by a measurable shear wave, was then tracked. The wave displacement phase images were recorded with a 256 × 256 acquisition matrix, two opposite polarities of the motion-encoding gradient with a 2.2 G/cm maximum amplitude limit, a flip angle of 45°, a 24 cm field of view, and a 5 mm slice thickness. Four offsets were recorded for the thigh muscles in a relaxed condition. The scan times at 70, 90, and 110 Hz were 38 seconds with TR/TE: 57.2/26.4 msec, 40 seconds with TR/TE: 55.6/23.2 msec, and 33 seconds with TR/TE: 54.6/21.2 msec, respectively.

PHANTOM CONFIGURATIONS. A phantom was placed inside the head coil of the MRI machine in a perpendicular direction to the static scanner field (B_0). A round pneumatic driver, based on the same principle as the silicone tube used for the muscle, was placed under the phantom to generate shear waves (Fig. 3a). The main vibration direction was perpendicular to the static B_0-field, and was propagated parallel to the axis of the phantom. Image slices were acquired in the coronal oblique plane to obtain vertical views through the phantom (Fig. 3b–d). Harmonic frequencies generated by the driver were performed at 60, 80, and 100 Hz. These frequencies are in the range of the optimal frequencies (from 60 to 100 Hz) previously defined for the use of this round driver.[11] A difference of 20 Hz was chosen between each frequency to visualize a variation of the wavelength. It should be noted that there is a discrepancy frequency between in vivo (70, 90, and 110 Hz) and in vitro (60, 80, and 100 Hz) studies. In both cases, low frequencies were applied and the purpose was not to compare in vivo and in vitro analysis at the same frequency, but to validate in vitro the postprocessing method before being applied in vivo. MRE acquisitions were performed with the following parameters: 256 × 256 matrix size, 200 × 200 mm field of view, 1.5 mm slice thickness, and four offsets for each frequency. TR/TE values

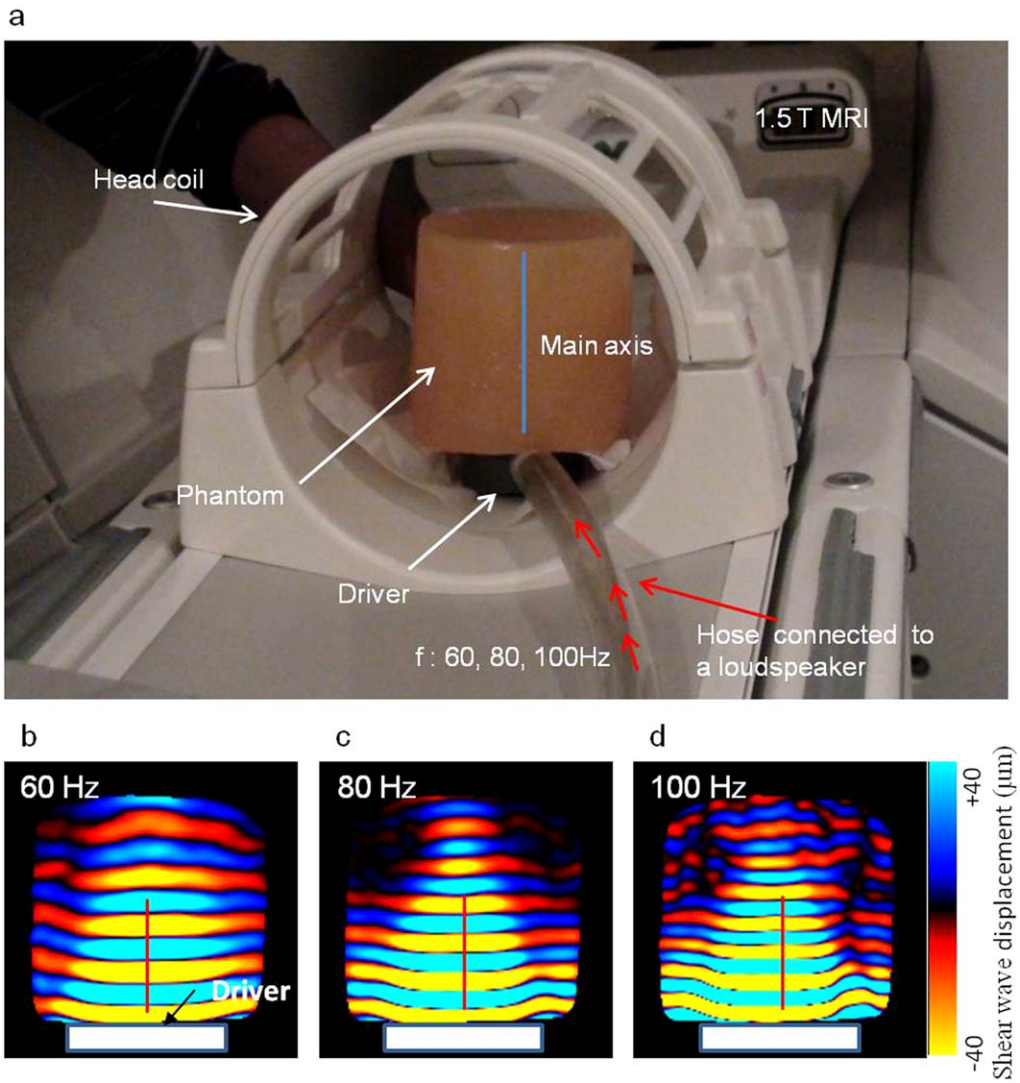

FIGURE 3: a: MMRE experimental set-up for the phantom. The wave's displacement inside the phantoms were generated at 60 Hz (b), 80 Hz (c), and 100 Hz (d) with a cylindrical driver by harmonic compression excitation.

at 60, 80, and 100 Hz were 66.7/27.7 msec, 62.5/33.4 msec, and 60.1/38.8 msec, respectively.

Data Processing

THEORY. Experimental ($\underline{G}(\omega)$) and numerical ($\underline{G}_{Model}(\omega)$) viscoelastic parameters were determined using basic equations that are summarized below.

A red profile (Figs. 2c, 5a) was prescribed in the direction (x) of the wave propagation, and the wave behavior along this profile was extracted (Fig. 5b). The amplitude of the wave along the profile was referred to as a scalar wave field $u(x, t)$ whose temporal Fourier-transformation was denoted $\underline{U}(x, w)$. Assuming that the medium of propagation was linear, locally homogeneous, isotropic, incompressible, and under pure shear stress, the motion equation (Helmholtz) in the frequency domain was [19]:

$$\rho\omega^2\underline{U}+\underline{G}(\omega)\frac{\partial^2}{\partial x^2}\underline{U}=0 \quad (1)$$

where $\omega = 2\pi f$ is the angular driving frequency, $\underline{G}(\omega) = G' + i\,G''$ is the complex shear modulus, and ρ is the muscle density.

It was assumed that the displacement of the wave followed a harmonic plane wave represented by the equation:

$$\underline{U}=u_0\exp[-i\underline{k}x] \quad (2)$$

where u_0 is the initial amplitude, and $\underline{k} = k - i\,\gamma$ is the complex wave number (k and γ are real parameters).

The parameter (k) was linked to the wavelength (λ) by the relationship $k = \frac{2\pi}{\lambda}$. The parameter (γ) corresponded to the attenuation coefficient. These two parameters were measured from the analysis of wave displacement $u(x, t)$ along the red profile (Fig. 5a). The wavelength (λ) was measured with the different extrema, and the corresponding location (x_i) was extracted from the wave (Fig. 5b). Two consecutive extrema were separated in (x) by a half period ($\frac{\lambda}{2}$). For better accuracy, the first and last extrema were used to deduce the value of λ (Fig. 5c). This process was applied to each offset and an average of the wavelength was determined.

Subsequently, a logarithmic $\ln(|U_i|)$ representation of the extrema was fitted with a linear least square line, which allowed measurement of the attenuation (γ) parameter (Fig. 5c). It can be noted that the slope of the line corresponded to $-\gamma$.

Solving Eq. (1) for $\underline{G}(\omega)$ with $\underline{U}$ from Eq. (2), and the parameters (k, γ), gave the following experimental viscoelastic parameters:

$$G'(\omega)=\rho\omega^2\frac{k^2-\gamma^2}{(k^2-\gamma^2)^2+(2k\gamma)^2} \quad (3)$$

$$G''(\omega)=\rho\omega^2\frac{2k\gamma}{(k^2-\gamma^2)^2+(2k\gamma)^2} \quad (4)$$

The complex modulus was related to elasticity (μ) and viscosity (η) using various rheological models. In this study, the four following models for $\underline{G}_M(\omega)$ were used:

$$\underline{G}_M(\omega)=\begin{cases}\mu+i\omega\eta & \text{Voigt}\\ \dfrac{i\omega\eta\mu}{\mu+i\omega\eta} & \text{Maxwell}\\ \dfrac{\mu_1\mu_2+i\omega\eta(\mu_1+\mu_2)}{\mu_2+i\omega\eta} & \text{Zener}\\ \mu^{1-\alpha}\eta^{\alpha}(i\omega)^{\alpha} & \text{Springpot}\end{cases} \quad (5)$$

Whereas the Voigt and Maxwell models require two parameters (μ: shear modulus and η: shear viscosity), the Zener (μ_1, μ_2, η) and springpot (μ, η, α) models take three parameters into account. Zener is similar to Hill's model representing the parallel elastic component ($\mu 1$) and the series elastic component ($\mu 2$) of the muscle structure. The parameter α represented a weighting factor between a purely elastic behavior ($\alpha = 0$) and a purely viscous behavior ($\alpha = 1$). For the springpot model, (μ) and (η) were linearly dependent, meaning that either the value of (μ) or (η) were fixed. Using the same assumption as in Klatt et al's study,[19] we fixed the η value to the data obtained in the Zener model.

The viscoelastic parameters (μ, η, α) from these four models were calculated by minimizing the following cost function (χ):

$$\chi=\frac{1}{N}\sum_{n=1}^{N}\sqrt{(\mathrm{Re}[\underline{G}(\omega_n)-\underline{G}_M(\omega_n)])^2+(\mathrm{Im}[\underline{G}(\omega_n)-\underline{G}_M(\omega_n)])^2} \quad (6)$$

where N is the number of experimental driving frequencies ($N = 3$).

IMAGE PROCESSING. The MMRE technique provides phase images, and presents the propagation of the shear wave within different muscles (SM, ST, BC, and Gr) at three different frequencies (Fig. 2c). Phase images were first unwrapped and filtered by a directional bandpass Butterworth filter to suppress the compression waves and to reduce noise.[35] Then the same operator manually drew a reference profile, within an accuracy of 5°, in the direction of the wave propagation within the four thigh muscles: Gr, SM, ST, and BC, to calculate the wavelength (λ) that represented the distance between consecutive peaks (Fig. 4). Subsequently, the complex shear modulus $\underline{G}(\omega)$ was calculated according to equations Eqs. (3) and (4), assuming a density of 1000 kg.m^{-3}. The rheological models were then estimated by minimizing Eq. (6). Three relative errors were also computed to compare the quality of fit across the driving frequencies:

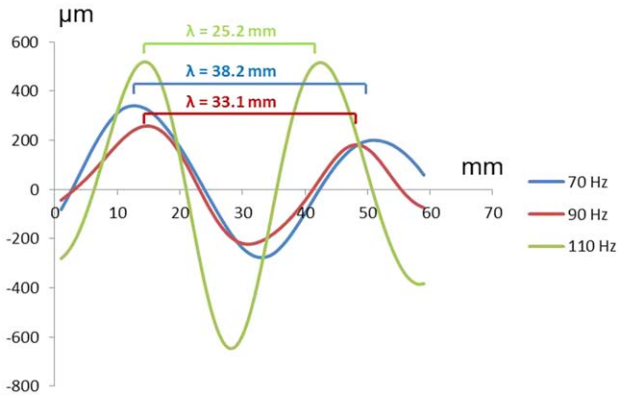

FIGURE 4: Representation of the wavelengths (λ) measured within the gracilis (Gr) muscle, along the red profile, for the three frequencies (70, 90, 110 Hz).

$$\chi_{\mathrm{fn}}=100\left|\frac{\sqrt{(\mathrm{Re}[\underline{G}_M(\omega_n)])^2+(\mathrm{Im}[\underline{G}_M(\omega_n)])^2}}{\sqrt{(\mathrm{Re}[\underline{G}(\omega_n)])^2+(\mathrm{Im}[\underline{G}(\omega_n)])^2}}-1\right| \quad (7)$$

where n = 1, 2, 3 ; $\omega_n = 2\pi f_n$; $f_1 = 70$ Hz; $f_2 = 90$ Hz; $f_3 = 110$ Hz.

Statistical Analyses

Analyses of variance (ANOVA) and Student's paired t-test were performed using Statgraphics 5.0 (Sigma Plus, Gaithersburg, MD) software to compare the viscoelastic parameter between muscles. The level of significance was set at $P < 0.1$ due to the low number of subjects.

Results

Phantom Measurements

Table 1 shows the results of the dynamic viscoelastic (G', G'') parameters measured experimentally with the Rheo-Spectris and MRE. Comparisons between the data revealed that the MRE technique underestimated the storage modulus (G') (min: 15.1%, max: 26%), whereas the loss modulus (G'') overestimated (min: 12%, max: 32%) the three frequencies. Moreover, the results of Bland–Altman test revealed that the differences of the viscoelastic parameters are in the range ±2 SD.

In Vivo Measurements

CHARACTERIZATION OF THE SHEAR WAVE WITHIN THE MUSCLES. Figure 2 shows clear and consistent displacement of the waves within the ischio (Fig. 2a) and gracilis (Fig. 2d) muscles. The same quality of propagation was obtained at all three frequencies (70, 90, 110 Hz). The placements of the imaging planes (dashed lines) were taken from a previous protocol that had been validated to characterize all the thigh muscles.[8] The present experimental MRE muscle protocol allowed propagation of the waves along a large piece of muscle (ie, along 20 cm of the Gr: Fig. 2f).

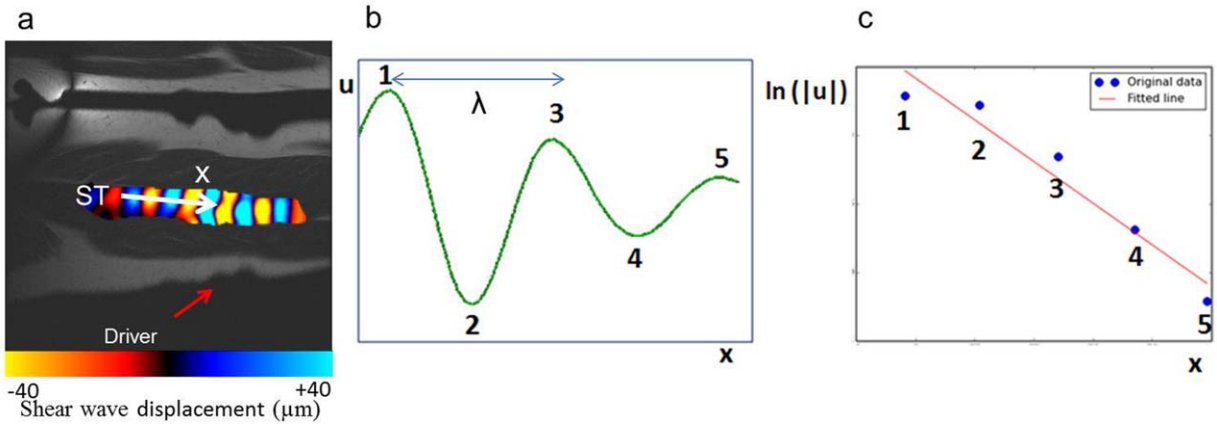

FIGURE 5: Illustration of the process to evaluate wave attenuation inside the semitendinous (ST). a: Phase image with a white profile, represented by an arrow, showing the direction of wave propagation inside the semitendinosus (ST). b: Amplitude of the wave along the profile as a function of distance, x. c: Plot of the extrema of the wave amplitude with the least-square fitted line to calculate the attenuation coefficient.

Figure 4 shows the behavior of the wavelength for the Gr muscle at the three frequencies. The wave was attenuated along its propagation and had a decreased wavelength (λ) (from 33.1 to 25.2 mm), in accordance with the increase in frequency. Similar results were obtained for the other muscles. When drawing each profile, care was taken to verify the validity of the waveform and ensure its attenuation value.

VISCOELASTIC PROPERTIES. Figure 6 presents the results of the experimental viscoelastic (G′ and G″) values for the three frequencies. The Gr muscle revealed higher elastic shear modulus (G′) values for the three frequencies compared to the other three muscles. In addition, the BC, SM, and ST had close shear moduli (G′) at 90 Hz. This result is likely related to the frequency, which has been previously demonstrated to be optimal at 90 Hz.[1] Both parameters (G′) and (G″) increased with frequency. The viscous shear modulus showed less variation compared to (G′) at each frequency, and between all the muscles. Consequently, the ratio of G″/G′ was similar (~0.3) at 70 and 90 Hz.

Table 2 shows the rheological fit for these parameters calculated with the Voigt, Maxwell, Zener, and springpot models, with data taken from the MRE viscoelastic parameters. The quality of fit was the best for the Zener model for each muscle. This result is represented by the lowest cost function error (χ) value found for this model. This finding supports the fact that the three-parameter Zener model was favored over a two-parameter model. Among the two-parameter models, the springpot also gave a low error value (χ).

Comparisons between the relative errors revealed that $\chi_{90\ Hz}$ was the smallest value compared to $\chi_{70\ Hz}$ and $\chi_{110\ Hz}$. This result was observed for all the models and all the muscles. It can be concluded that the experimental data obtained at 90 Hz gave the best agreement with the rheological models.

According to the parameters from the rheological model (Table 2), the Zener and springpot models were further compared to muscle viscoelasticity. Figure 7 shows the results obtained with the Zener model. We recall that ($\mu 1$) is related to the elasticity of a spring element that is parallel to the Maxwell elements, which is composed of an elastic ($\mu 2$) and a viscous (η) component. For the elastic component ($\mu 1$) (Fig. 7b), it appeared that the Gr muscle (μ_{1_Gr} = 5.20 ± 1.26 kPa) was significantly different from the BC (μ_{1_BC} = 3.42 ± 0.45 kPa), SM (μ_{1_SM} = 2.92 ± 0.41 kPa), and ST (μ_{1_ST} = 3.92 ± 0.44 kPa). The Gr muscle also showed similar greater elastic behavior than the experimental (G′) at 90 Hz (Fig. 6a). The values of Zener's second elastic component (μ_2) were higher than those for (μ_1) for BC, SM, and ST. However, the values of (μ_2) between

TABLE 1. Dynamic Experimental Viscoelastic Parameters (G′, G″) Measured With a Rheospectris and MRE Techniques at Three Drive Frequencies (Mean ± SEM).

Method	Parameter	60 Hz	80 Hz	100 Hz
RheoSpectris	G′ (kPa)	1.835 ± 0.001	1.843 ± 0.001	1.853 ± 0.001
	G″ (kPa)	0.1902 ± 0.0004	0.2530 ± 0.0005	0.3154 ± 0.0006
MR elastography	G′ (kPa)	1.358 ± 0.013	1.579 ± 0.004	1.574 ± 0.015
	G″ (kPa)	0.2129 ± 0.0092	0.3319 ± 0.0016	0.4162 ± 0.0247

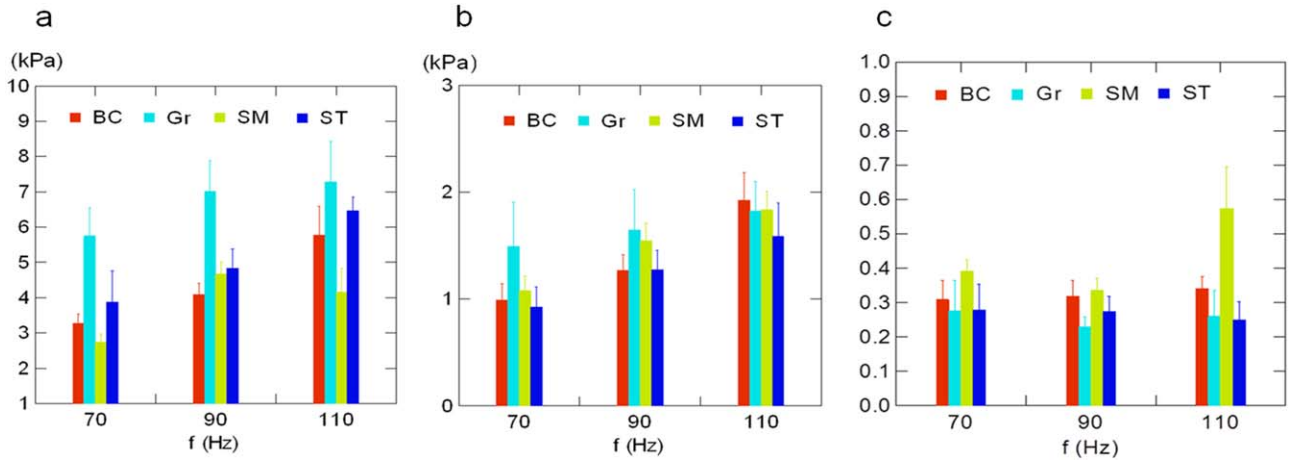

FIGURE 6: Mean ± SEM of the dynamic experimental viscoelastic parameters (a: G′, b: G″ and c: G″/G′) measured with MRE at the three drive frequencies for the semimembranosus (SM), semitendinosus (ST), biceps (BC), and gracilis (Gr) muscles.

muscles were not statistically different. Concerning the viscous component (η), a similar range of values was obtained for BC, SM, and ST, with the Gr showing higher values that were not significantly different from those of the other muscles.

Concerning the springpot model (Fig. 8), significant higher values of (μ) were observed for the Gr muscle (μ = 8.1 ± 1.8 kPa) compared to the other muscles. This result was similar to the experimental elastic shear modulus obtained at 90 Hz (Fig. 6a). Concerning the α values, the SM muscle had a higher (α = 0.266 ± 0.023) value compared to the other muscles (Fig. 8a). Moreover, the trend of α values for each muscle was equivalent to that obtained for the ratio G″/G′ at 90 Hz (Fig. 6c).

Discussion

The novelty of the present study is its direct method to extract the in vivo viscoelastic parameters from experimental wavelength and attenuation measurements. This data processing was validated first on phantoms before being applied to muscles. Indeed, it was demonstrated that the experimental G′ and G″ values provided by the hyperfrequency viscoelastic spectroscopy technique are in agreement with those measured by our method using multifrequency MRE tests. Moreover, our approach was based on a profile placed within the region of interest on the muscle and within the direction of wave propagation. This made the present method more sensitive to changes in the muscle's mechanical properties. Another advantage of our method was that it did not need to calculate the Laplacian operator ($\frac{\partial^2}{\partial x^2}\underline{U}$) in Eq. (1). Only the locations of the extrema in the waveform were needed.

In this study, our approach was based on the local homogeneity of the biological tissue by local measurement along the profile: thus we assumed that the spatial derivatives of shear modulus ($\frac{\partial}{\partial x}\underline{G}$) were negligible.[34] A more realistic model for muscle tissue may have used the assumption of a transversely isotropic and incompressible medium.[34,36] In the case of compressibility, the Helmholtz equation (Eq. (1)) must be corrected by an additional term for pressure,[37] which requires the acquisition of a 3D MR phase image to calculate the curl operator. In addition, a transversely isotropic medium assumes reconstructing two shear moduli (parallel and perpendicular to the muscle fibers) with a diffusion tensor imaging sequence.[34] Muscle is a complex biological tissue composed of multiple parameters, which need to all be taken into account but which is not compatible with general clinical investigations due to the increase times of MR acquisition.

This study focused on four relaxed healthy muscles (BC, Gr, SM, ST) and is a follow-on study on work in which we quantified the passive elastic properties of nine thigh muscles.[8] The present results have extended this previous database using passive viscoelastic data from MMRE tests. Comparison of viscoelastic measurements with other studies on muscles is difficult because of the different experimental setups and methods of data processing. Moreover, some studies have characterized isolated muscles, such as the vastus medialis and sartorius,[38] whereas others have measured the viscoelastic properties of a group of femoral muscles.[19] For instance, Klatt et al's study used the same criterion of fit (Eq. (6)) as in our present study, but the MMRE tests were performed at a lower frequency range (25–62.5 Hz), with a shear motion driver, and a group of femoral muscles were analyzed. As a consequence, comparisons of the elastic values obtained with the springpot model for the BC (μ = 5.65 ± 0.33 kPa), Gr (μ = 8.10 ± 0.80 kPa), SM (μ = 5.30 ± 0.29 kPa), and ST (μ = 6.10 ± 0.38 kPa) muscles are not within same range as in Klatt et al's study for the femoral muscle (μ= 2.68 ± 0.23 kPa).

Another example is Debernard et al's study,[38] where they used the same driver frequencies for the MMRE tests

TABLE 2. Rheological Model Parameters (Mean ± SEM) and Error of the Fit Measured From MMRE Tests Realized From Four Thigh Muscles

Model	Parameter	BC	Gr	SM	ST
Voigt	η (Pa s)	2.51 ± 0.18	2.85 ± 0.27	2.93 ± 0.24	2.20 ± 0.17
	μ (kPa)	4.38 ± 0.26	6.88 ± 0.78	3.86 ± 0.22	5.00 ± 0.40
	χ (kPa)	0.35 ± 0.11	0.46 ± 0.13	0.42 ± 0.10	0.41 ± 0.10
	$\chi_{70\ Hz}$ (%)	12.9 ± 7.6	11.8 ± 5.9	17.3 ± 9.3	9.9 ± 4.4
	$\chi_{90\ Hz}$ (%)	7.5 ± 1.1	7.3 ± 1.3	12.5 ± 4.3	8.5 ± 3.5
	$\chi_{110\ Hz}$ (%)	14.0 ± 2.5	9.6 ± 1.6	22.5 ± 5.8	13.7 ± 3.3
Maxwell	η (Pa s)	25.35 ± 1.41	55.10 ± 8.71	18.60 ± 1.04	40.27 ± 9.79
	μ (kPa)	4.90 ± 0.30	7.32 ± 0.79	4.62 ± 0.31	5.42 ± 0.34
	χ (kPa)	0.41 ± 0.09	0.49 ± 0.09	0.46 ± 0.09	0.42 ± 0.09
	$\chi_{70\ Hz}$ (%)	12.7 ± 7.7	11.6 ± 6.0	16.1 ± 9.1	10.0 ± 4.5
	$\chi_{90\ Hz}$ (%)	7.3 ± 1.5	6.9 ± 1.1	12.3 ± 4.6	8.7 ± 3.9
	$\chi_{110\ Hz}$ (%)	13.3 ± 2.6	9.2 ± 1.2	22.7 ± 6.8	13.2 ± 3.3
Zener	η (Pa s)	3.96 ± 0.54	6.65 ± 1.47	4.19 ± 0.39	4.29 ± 0.81
	μ_1 (kPa)	3.42 ± 0.20	5.20 ± 0.56	2.92 ± 0.18	3.92 ± 0.44
	μ_2 (kPa)	6.90 ± 3.28	6.36 ± 2.63	7.38 ± 3.22	3.34 ± 0.21
	χ (kPa)[a]	**0.31 ± 0.08**	**0.37 ± 0.08**	**0.38 ± 0.09**	**0.35 ± 0.08**
	$\chi_{70\ Hz}$ (%)	10.9 ± 6.0	9.97 ± 4.81	14.1 ± 7.4	8.2 ± 3.4
	$\chi_{90\ Hz}$ (%)	7.8 ± 1.6	7.15 ± 1.33	12.6 ± 4.4	9.3 ± 3.9
	$\chi_{110\ Hz}$ (%)	11.9 ± 1.5	7.77 ± 1.35	22.0 ± 6.3	11.4 ± 2.6
springpot	η (Pa s)	3.96 ± 0.54	6.65 ± 1.47	4.19 ± 0.39	4.29 ± 0.81
	μ (kPa)	5.65 ± 0.33	8.10 ± 0.80	5.30 ± 0.29	6.10 ± 0.38
	α	0.210 ± 0.009	0.158 ± 0.012	0.266 ± 0.010	0.172 ± 0.022
	χ (kPa)	0.35 ± 0.08	0.44 ± 0.09	0.42 ± 0.09	0.38 ± 0.08
	$\chi_{70\ Hz}$ (%)	13.5 ± 6.5	11.1 ± 4.9	16.5 ± 8.4	9.3 ± 3.3
	$\chi_{90\ Hz}$ (%)	7.7 ± 1.6	7.3 ± 1.3	12.5 ± 4.2	8.7 ± 3.7
	$\chi_{110\ Hz}$ (%)	13.4 ± 1.6	8.8 ± 1.8	23.3 ± 6.2	13.0 ± 3.0

BC: biceps; Gr: Gracilis; SM: semimembranosus; ST: semitendinosus; η: viscosity; μ: elasticity; α: viscoelastic constant.
[a]The minimum cost function error χ values are represented in bold.

as in our present study, but their fit of the rheological model differed to ours. Theirs was based on a cost function composed of the speed of the experimental shear wave, whereas we used the experimental wavelength and attenuation to measure (G′) and (G″) (Eq. (6)). Even though comparisons could be biased, the viscosities (η, Zener) of the vastus medialis (3.57 ± 0.92 Pa.s) and sartorius (6.37 ± 1.13 Pa.s), as reported by Debernard et al, were within the same range as for BC (3.96 ± 0.54 Pa.s), SM (4.19 ± 0.39 Pa.s), ST (4.29 ± 0.81 Pa.s), and Gr (6.61 ± 1.47 Pa.s).

Comparison between the Zener and springpot models showed a similar behavior regarding the elastic components for each muscle. The Gr muscle showed higher elastic values in both models compared to the other muscles. This has been reported previously[1] and additional spectroscopic investigations are needed to further characterize the structural properties that explain this higher elasticity. The μ_1 parameter from the Zener model could be a marker of the passive function (conjunctive tissue, sarcolemma, etc.) and the variation of $\mu 1$ data could represent different muscle passive behaviors. The $\mu 2$ parameter shows the active part (actin myosin bands) and the no significant difference of $\mu 2$ data, between the four muscles, could be due to the passive condition tested in this study.

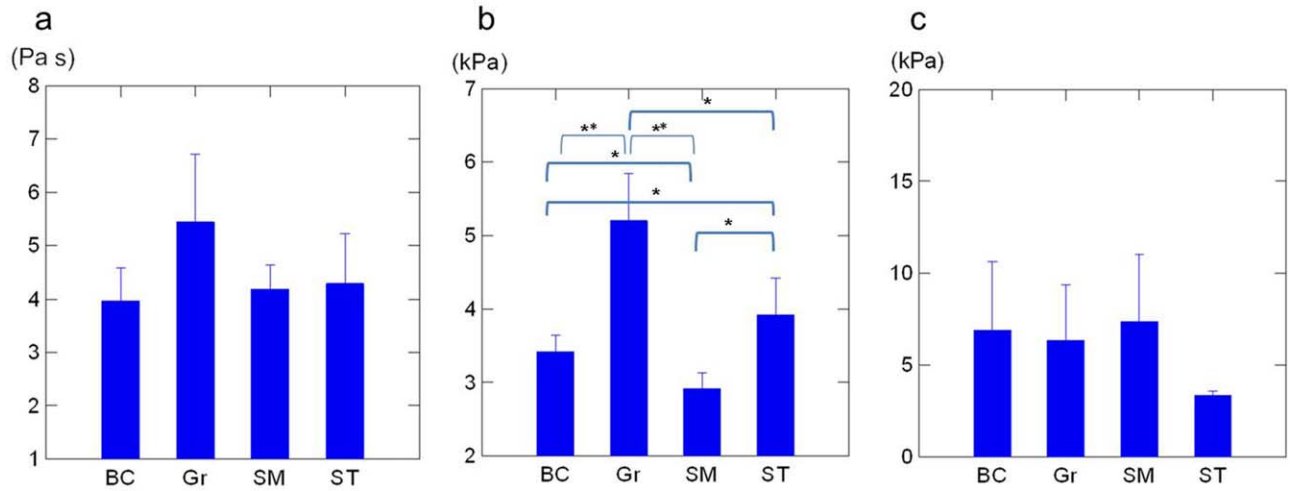

FIGURE 7: Mean ± SEM of the viscoelastic parameters. a: viscosity (η). b: elasticity (μ_1). c: elasticity (μ_2) of the four thigh muscles (semimembranosus (SM), semitendinosus (ST), biceps (BC), and gracilis (Gr) muscles) obtained from the Zener model. ($P < 0.05$, *$P < 0.1$).**

The springpot model also provided an insight into muscle physiology.[19,49] Indeed, it is known that the parameter α is determined by the degree of freedom in the underlying network of tissue.[40] Thus, the low α-value (0.155) for the phantom revealed a homogeneous media, which is in agreement with the uniform preparation of the phantom. It can be noted that this α value was close to those obtained for the Gr and ST muscles. Higher α values were calculated for BC (0.210 ± 0.020) and SM (0.266 ± 0.023) muscles, whereas Gr (0.158 ± 0.012) and ST (0.172 ± 0.022) muscles had significantly lower values. These results indicate a more hierarchical structure for BC and SM muscles, represented by the presence of more cross-bridges between muscle filaments at the microstructural level. Moreover, the Gr and ST do not have well-formed tendons in the mid-thigh compared to the BC and SM muscles. Thus, this difference between the muscles could be linked to more complex muscle architecture relative to the tendon. This range of values was also found by Klatt et al's study[19] for the femoral muscles (0.253 ± 0.009). In addition, the trend of α values for each muscle was similar to the experimental ratio G''/G' at 90 Hz. This last result demonstrates that the optimal frequency to characterize muscle using MMRE with the tube driver is 90 Hz. This statement is in agreement with previous experimental muscle studies.[10,27]

In conclusion, the present MMRE tests associated with the data-processing method showed that the complex shear modulus of passive muscle can be analyzed using two rheological models (Zener, springpot). The elastic and viscous data could be used as a reference for future assessment of muscular dysfunction in addition to the parameters related to the aging process and anthropometry. Further

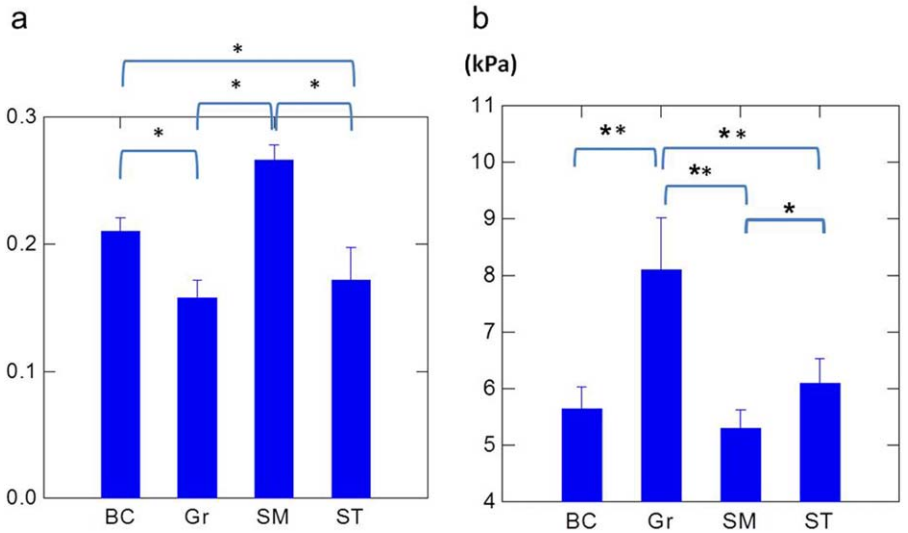

FIGURE 8: Comparison of the viscoelastic parameters (mean ± SEM) a: viscoelastic constant α; b: elasticity (μ) of the four thigh muscles (semimembranosus (SM), semitendinosus (ST), biceps (BC), and gracilis (Gr) muscles) obtained from the springpot model. ($P < 0.05$, *$P < 0.1$).**

experiments will be performed on a much larger number of participants and on the other thigh muscles under active conditions in order to obtain a complete muscle database of their functional properties.

Acknowledgments

We thank Dr. R.L. Ehman at the Mayo Clinic, Department of Radiology, for MR support technology. We thank the Rheolution company for the tests performed on the samples with the RheoSpectris C500 instrument.

Author Contributions

Conceived and designed the experiments: MKC, FC, SFB. Wrote the article: MKC, PP, SFB. Performed the experiments: MKC, FC, SFB. Analyzed the data: MKC, PP, SFB. Contributed reagents/materials/analysis tools: MKC, PP, SFB. Contributed to the revision of the article: MKC, PP, FC, SFB.

References

1. Bensamoun SF, Ringleb SI, Chen Q, Ehman RL, An K-N, Brennan M. Thigh muscle stiffness assessed with magnetic resonance elastography in hyperthyroid patients before and after medical treatment. J Magn Reson Imaging 2007;26:708–713.
2. Brauck K, Galban CJ, Maderwald S, Herrmann BL, Ladd ME. Changes in calf muscle elasticity in hypogonadal males before and after testosterone substitution as monitored by magnetic resonance elastography. Eur J Endocrinol 2007;156:673–678.
3. Muthupillai R, Lomas D, Rossman P, Greenleaf J, Manduca A, Ehman R. Magnetic resonance elastography by direct visualization of propagating acoustic strain waves. Science 1995;269:1854–1857.
4. Green MA, Geng G, Qin E, Sinkus R, Gandevia SC, Bilston LE. Measuring anisotropic muscle stiffness properties using elastography. NMR Biomed 2013;26:1387–1394.
5. Bilston LE, Tan K. Measurement of passive skeletal muscle mechanical properties in vivo: recent progress, clinical applications, and remaining challenges. Ann Biomed Eng 2014;1–13.
6. Bensamoun SF, Robert L, Leclerc GE, Debernard L, Charleux F. Stiffness imaging of the kidney and adjacent abdominal tissues measured simultaneously using magnetic resonance elastography. Clin Imaging 2011;35:284–287.
7. Venkatesh SK, Yin M, Glockner JF, et al. MR elastography of liver tumors: preliminary results. Am J Roentgenol 2008;190:1534–1540.
8. Chakouch MK, Charleux F, Bensamoun SF. Quantifying the elastic property of nine thigh muscles using magnetic resonance elastography. PloS One 2015;10:e0138873.
9. Klatt D, Hamhaber U, Asbach P, Braun J, Sack I. Noninvasive assessment of the rheological behavior of human organs using multifrequency MR elastography: a study of brain and liver viscoelasticity. Phys Med Biol 2007;52:7281–7294.
10. Debernard L, Leclerc GE, Robert L, Charleux F, Bensamoun SF. In vivo characterization of the muscle viscoelasticity in passive and active conditions using multifrequency MR elastography. J Musculoskelet Res 2013;16:1350008.
11. Leclerc GE, Charleux F, Robert L, et al. Analysis of liver viscosity behavior as a function of multifrequency magnetic resonance elastography (MMRE) postprocessing. J Magn Reson Imaging 2013;38:422–428.
12. Green MA, Bilston LE, Sinkus R. In vivo brain viscoelastic properties measured by magnetic resonance elastography. NMR Biomed 2008; 21:755–764.
13. Hirsch S, Guo J, Reiter R, et al. MR elastography of the liver and the spleen using a piezoelectric driver, single-shot wave-field acquisition, and multifrequency dual parameter reconstruction: multi-frequency MR elastography of the liver and the spleen. Magn Reson Med 2014; 71:267–277.
14. Catheline S, Gennisson J-L, Delon G, et al. Measurement of viscoelastic properties of homogeneous soft solid using transient elastography: an inverse problem approach. J Acoust Soc Am 2004;116: 3734–3741.
15. Chen S, Urban MW, Pislaru C, et al. Shearwave dispersion ultrasound vibrometry (SDUV) for measuring tissue elasticity and viscosity. IEEE Trans Ultrason Ferroelectr Freq Control 2009;56:55–62.
16. Gennisson J-L, Deffieux T, Macé E, Montaldo G, Fink M, Tanter M. Viscoelastic and anisotropic mechanical properties of in vivo muscle tissue assessed by supersonic shear imaging. Ultrasound Med Biol 2010;36:789–801.
17. Oliphant TE, Manduca A, Ehman RL, Greenleaf JF. Complex-valued stiffness reconstruction for magnetic resonance elastography by algebraic inversion of the differential equation. Magn Reson Med 2001;45: 299–310.
18. Papazoglou S, Hamhaber U, Braun J, Sack I. Algebraic Helmholtz inversion in planar magnetic resonance elastography. Phys Med Biol 2008;53:3147.
19. Klatt D, Papazoglou S, Braun J, Sack I. Viscoelasticity-based MR elastography of skeletal muscle. Phys Med Biol 2010;55:6445–6459.
20. Meyers MA, Chawla KK. Mechanical behavior of materials, 2nd ed. Cambridge, New York: Cambridge University Press; 2009.
21. Ringleb SI, Chen Q, Lake DS, Manduca A, Ehman RL, An K-N. Quantitative shear wave magnetic resonance elastography: comparison to a dynamic shear material test. Magn Reson Med 2005;53:1197–1201.
22. Manduca A, Oliphant TE, Dresner MA, et al. Magnetic resonance elastography: non-invasive mapping of tissue elasticity. Med Image Anal 2001;5:237–254.
23. Drapaca CS. A novel mechanical model for magnetic resonance elastography. Rev Roum Sci Tech 2010;38:3–18.
24. Numano T, Kawabata Y, Mizuhara K, Washio T, Nitta N, Homma K. Magnetic resonance elastography using an air ball-actuator. Magn Reson Imaging 2013;31:939–946.
25. Chen Q, Bensamoun S, Basford JR, Thompson JM, An K-N. Identification and quantification of myofascial taut bands with magnetic resonance elastography. Arch Phys Med Rehabil 2007;88:1658–1661.
26. Kolipaka A, McGee KP, Manduca A, et al. Magnetic resonance elastography: inversions in bounded media. Magn Reson Med 2009;62: 1533–1542.
27. Leclerc GE, Debernard L, Foucart F, et al. Characterization of a hyperviscoelastic phantom mimicking biological soft tissue using an abdominal pneumatic driver with magnetic resonance elastography (MRE). J Biomech 2012;45:952–957.
28. Oudry J, Lynch T, Vappou J, Sandrin L, Miette V. Comparison of four different techniques to evaluate the elastic properties of phantom in elastography: is there a gold standard? Phys Med Biol 2014;59:5775–5793.
29. Oudry J, Bastard C, Miette V, Willinger R, Sandrin L. Copolymer-in-oil phantom materials for elastography. Ultrasound Med Biol 2009;35: 1185–1197.
30. Suzuki H, Tadano S, Goto M, et al. Viscoelastic modulus of agarose gels by magnetic resonance elastography using Micro-MRI. Mech Eng J 2015 [Epub ahead of print].
31. Hadj Henni A, Schmitt C, Tremblay M-É, et al. Hyper-frequency viscoelastic spectroscopy of biomaterials. J Mech Behav Biomed Mater 2011;4:1115–1122.
32. Chakouch MK, Charleux F, Bensamoun SF. Development of a phantom mimicking the functional and structural behaviors of the thigh

muscles characterized with magnetic resonance elastography technique. Milano Conference Center, Milan, Italy, August 25-29 2015 [Epub ahead of print].

33. Altman DG, Bland JM. Measurement in medicine: the analysis of method comparison studies. J R Stat Soc Ser Stat 1983;32:307–317.

34. Sinkus R, Tanter M, Catheline S, et al. Imaging anisotropic and viscous properties of breast tissue by magnetic resonance-elastography. Magn Reson Med 2005;53:372–387.

35. Manduca A, Lake DS, Kruse SA, Ehman RL. Spatio-temporal directional filtering for improved inversion of MR elastography images. Med Image Anal 2003;7:465–473.

36. Qin EC, Sinkus R, Rae C, Bilston LE. Investigating anisotropic elasticity using MR-elastography combined with diffusion tensor imaging: validation using anisotropic and viscoelastic phantoms. In: Proc 19th Annual Meeting ISMRM, Montreal; 2011:39.

37. Sinkus R, Daire J-L, Van Beers BE, Vilgrain V. Elasticity reconstruction: beyond the assumption of local homogeneity. Compt Rend Mécan 2010;338:474–479.

38. Debernard L, Robert L, Charleux F, Bensamoun SF. Analysis of thigh muscle stiffness from childhood to adulthood using magnetic resonance elastography (MRE) technique. Clin Biomech 2011;26:836–840.

39. Anantawaraskul S. Polymer analysis/polymer theory. Springer Science & Business Media; 2005.

40. Gurtovenko AA, Blumen A. Generalized Gaussian structures: models for polymer systems with complex topologies. In: Advances in polymer science, vol. 182. Berlin, Heidelberg: Springer; 2005. p 171–282.